Articles

Active Serine Involved in the Stabilization of the Active Site Loop in the *Humicola lanuginosa* Lipase†

G. H. Peters,*,‡,⊥ A. Svendsen,§ H. Langberg,§ J. Vind,§ S. A. Patkar,§ S. Toxvaerd,‡ and P. K. J. Kinnunen||

Chemistry Department III, H.C. Ørsted Institutet, University of Copenhagen, Universitetsparken 5, DK-2100 Copenhagen Ø, Denmark, Novo-Nordisk A/S, Novo Allé 1, DK-2880 Bagsvaerd, Denmark, and Department of Medical Chemistry, Institute of Biomedicine, University of Helsinki, Helsinki, Finland

Received November 25, 1997; Revised Manuscript Received April 1, 1998

ABSTRACT: We have investigated the binding properties of and dynamics in *Humicola lanuginosa* lipase (Hll) and the inactive mutant S146A (active Ser146 substituted with Ala) using fluorescence spectroscopy and molecular dynamics simulations, respectively. Hll and S146A show significantly different binding behavior for phosphatidylcholine (PC) and phosphatidylglycerol (PG) liposomes. Generally, higher binding affinity is observed for Hll than the S146A mutant. Furthermore, depending on the matrix, the addition of the transition state analogue benzene boronic acid increases the binding affinity of S146A, whereas only small changes are observed for Hll suggesting that the active site lid in the latter opens more easily and hence more lipase molecules are bound to the liposomes. These observations are in agreement with molecular dynamics simulations and subsequent essential dynamics analyses. The results reveal that the hinges of the active site lid are more flexible in the wild-type Hll than in S146A. In contrast, larger fluctuations are observed in the middle region of the active site loop in S146A than in Hll. These findings reveal that the single mutation (S146A) of the active site serine leads to substantial conformational alterations in the *H. lanuginosa* lipase and different binding affinities.

In recent years the three-dimensional structures of several microbial lipases (acylglycerol acylhydrolase, EC 3.1.1.3) have been determined by X-ray crystallographic methods (*1*, *2*) including wild-type lipases and lipase−inhibitor complexes (active conformers). The *Rhizomucor miehei* lipase−inhibitor complex was the first structure to be crystallographically resolved (*2*−*4*). This structure provided insight into the molecular basis of the catalytic function and revealed that the catalytic center consists of a triad [Ser···His···acidic residue]. In the native conformation, the active site is shielded from the solvent by an α-helical loop ("lid"), which upon activation of the lipase is displaced to allow access of the substrate to the active site. When compared with the closed conformations of these enzymes, all active conformers expose large hydrophobic surfaces which probably interact favorably with a lipid interface (*5*). For example, upon activation of *R. miehei* lipase the accessible hydrophobic surface increases by approximately 750 Å^2 (*4*). As the lid rolls over, polar residues on the α-helix and on the surface adjacent to it become buried. At the same time, water molecules, which in the wild-type enzyme form a well-defined network on the polar surface, are displaced. The activation and subsequent binding of lipases toward a lipid interface are complex processes. The free-energy changes involved in these processes are caused by various contributions such as hydrogen bonding, van der Waals and electrostatic interactions, solvation and hydrophobic interactions, and entropies due to translations, vibrations, rotations, and configurational changes (*6*−*10*). The free-energy change associated with the removal of polar residues and the exposure of apolar residues is highly dependent on the structural details of the lipid interface (*6*, *7*). Experimentally, it has been observed that in an aqueous solution, the lipase activity is increased in the presence of a lipid interface (*11*). In solution, the opening of the lid is presumably thermodynamically unfavorable, because of a large hydrophobic patch that would necessarily be exposed to the polar solvent as a result. Conversely, in the presence of hydrophobic interfaces, the nonpolar surface would be favored, and hence the open conformation of the lid would be stabilized (*9*, *12*).

Despite the understanding of the mechanistic basis of their catalytic function, many of the factors influencing lipase activity are still not well understood. Lipases display a much higher activity on lipid aggregates, such as micelles or lipid bilayers, compared with the enzyme acting on lipid monomers in aqueous solution. The interfacial catalysis involves

† Financial support from the European Biotechnology Organization (Grant BIOZ-CT93-5507) and the European Molecular Biology Organization (EMBO) (Grant ASTF 8302) is gratefully acknowledged.

* To whom correspondence should be addressed. Phone: (+45) 35320236. Fax: (+45) 35320259. E-mail: ghp@st.ki.ku.dk.

‡ University of Copenhagen.

§ Novo-Nordisk A/S.

|| University of Helsinki.

⊥ Current address: Department of Chemistry, Technical University of Denmark, Building 206, DK-2800 Lyngby, Denmark.

S0006-2960(97)02883-3 CCC: $15.00
Published on Web 08/18/1998

a series of reaction steps (such as binding to the lipid surface, activation of the enzyme, penetration into the lipid phase, and catalytic hydrolysis) that require a specific kinetic analysis beyond conventional schemes (*13*). Many mechanisms have been proposed to explain the activation of lipases at a lipid−water interface including an increase of substrate concentration at the interface, better orientation of the scissile ester bond, reduction in the water shell around the ester molecules in water, and a conformational change in the enzyme. Theories describing the enzymatic process are based on either the "substrate theory" or the "enzyme theory" (*1*, *14*−*16*). The substrate theory assumes that preexisting structural ordering of the lipid and/or lipid−water interface may govern the biochemical activity. The enzyme theory suggests that the conformational changes in the enzyme upon adsorption onto the interface determine the lipase action. Hence, the biochemical activities are controlled by structural changes and/or by changes in the motion of flexible loops in the enzymes (*17*−*20*). As shown by earlier studies, these models are merely conceptual extremes and are not mutually exclusive (*15*, *21*, *22*). Due to the experimental difficulties in obtaining detailed information (at the molecular level) about the lipid environment and its influence on lipid−enzyme interactions, there is still a gap in correlating the enzyme activity to the interfacial properties of the lipid substrate. X-ray diffraction data provide important, but predominantly static, information about lipase structures. In solution, the motion of the enzyme is probably complex, and in particular, as the enzyme approaches the substrate, lipid−enzyme interactions may play an important role in the activation process.

To establish a link between substrate properties and the lipase action, we have investigated the binding affinity of Hll[1] and its inactive mutant (S146A). Binding affinities were deduced from fluorescence spectroscopy measurements, while protein dynamics was derived from molecular dynamics simulations. The results obtained with both techniques indicate that protein flexibility could alter the binding properties of proteins.

MATERIALS AND METHODS

Cloning and Expression of Lipases. The gene from *Humicola lanuginosa* encoding the triglyceride lipase was cloned, sequenced, and expressed as described earlier (*23*), and the lipase produced was isolated from the culture medium. The S146A mutant was transformed into *Aspergillus oryzae* and fermented as mentioned in ref *24*.

Site-Directed Mutagenesis. The method and procedure used for the mutation of the lipase gene has been described earlier (*23*, *26*). The correct mutation was verified by DNA sequencing.

Lipase Purification. The produced wild-type and mutated lipases were purified by a procedure containing two chromatographic steps. (i) Hydrophobic interaction chromatography: A 50 mL column was packed with Butyl Toyopearl matrix (*27*) as described by the manufacturer. The column was then equilibrated with 0.8 M ammonium acetate at a flow rate of 5 mL/min and was washed until OD280 was below 0.05. Bound enzyme was eluted with Milli-Q water (18 M ohm cm). The fractions with lipase activity were pooled, and the solutions were adjusted to pH 7 and to a conductance of 2 mSi using Milli-Q water. (ii) Ion-exchange chromatography on fast-flow Q sapphires: A 50 mL prefaced column from Pharmacy Biotech was equilibrated with 50 mM borate pH 8. The lipase solutions were then applied on the prepacked column and washed until no UV absorbing impurities could be detected in the fractions. Bound lipase was eluted with a linear salt gradient up to 1 M NaCl in borate buffer (pH 8) at a flow rate of 1 mL/min. No contaminants could be detected in the purified lipase after sodium dodecyl sulfate−polyacrylamide gel electrophoresis (SDS−PAGE).

Assay. Wild-type lipase was assayed by using tributyrin as the substrate and gum arabic as the emulsifier as described in ref *23*. Active site variant (S146A) was assayed applying Rocket immunoelectrophoresis and using antibodies raised against the lipase.

Lipase Quantitation. Protein concentrations were determined spectrophotometrically at 280 nm (extinction coefficient, $\epsilon = 43\,000$ L/(mol cm)).

Labeling of Hll with FITC. Hll was labeled with fluorescein 5-isothiocyante (FITC) using the procedure described in ref *25*. Lipase (15 mg) was dissolved in 3 mL of 50 mM sodium phosphate buffer adjusted to pH 9.5 with 5 N NaOH; 0.1 mL of ethanoic FITC solution (6.2 mM) was added to the solution resulting in a FITC/Hll molar ratio of 4.0. The mixture was incubated for 3 h in the dark at room temperature with occasional shaking. The reaction was stopped by adjusting the pH of the reaction mixture to 6.0 with diluted HCl solution. The solution was then dialyzed with 2 L of a high ionic strength buffer composed of 0.6 M NaCl and 10 mM Tris (pH = 7.0) to remove unreacted FITC. The buffer was changed after 1, 2, 4, and 8 h. The protein solution was desalted by dialysis against 20 mM Hepes buffer containing 0.1 mM EDTA (pH = 7.4). The amount of FITC bound to Hll was determined by light absorption at 500 nm using a molar extinction coefficient of $\epsilon = 76\,000$ L/(mol cm) (*28*). The protein concentration was determined by the method of Bradford (*29*). The lipase/FITC molar ratios were 4.9 and 2.7 for the wild-type and the S146A mutant, respectively.

Preparation of Liposomes. Appropriate amounts of phospholipids and pyrene-labeled phospholipids in chloroform were mixed to yield the desired molar ratio. Chloroform was then evaporated under a stream of nitrogen, and the remaining lipids were kept under high vacuum for at least 2 h. The lipid was hydrated with 20 mM Hepes buffer containing 0.1 mM EDTA (pH 7.4) for 45 min at room temperature with occasional shaking. The multilamellar vesicles were extruded through 100 nm polycarbonate filters (PM-10, $d = 43$ mm, WA AE cgu 6D, see ref *30*), which were mounted in a mini-extruder fitted with two 0.25 mL Hamilton syringes (*31*). The samples were subjected to 19 passes through two filters in tandem. The phospholipid/pyrene-labeled phospholipid molar ratio in the liposomes was 3.18, if not indicated otherwise.

[1] Abbreviations: BBA, benzene boronic acid; bisPDPC, 1-palmitoyl-2(pyren-1-yl)decanoyl-*sn*-glycero-3-phosphatidylcholine; bisPDPG, 1-palmitoyl-2(pyren-1-yl)decanoyl-*sn*-glycero-3-phosphatidylglycerol; DMPC, 1,2-dimyristoyl-*sn*-glycero-3-phosphocholine; DMPG, 1,2-dimyristoyl-*sn*-glycero-3-phosphoglycerol; Hll, *Humicola lanuginosa* lipase; S146A, mutant of *Humicola lanuginosa* lipase (active Ser146 substituted with Ala).

Fluorescence Measurements. Fluorescence intensities were measured using an SLM-4800S spectrofluorometer (*32*) equipped with a magnetically stirred thermostated compartment. Two different approaches were used to determine the binding properties of Hll and its inactive mutant (S146A): (i) For tryptophan fluorescence, the samples were excited at 290 nm and the emission intensity was measured at 377 nm. A cuvette with 2 mL of buffer containing 3.8 μM enzyme was placed in the spectrometer and liposomes were continuously added to the solution. (ii) For FITC fluorescence, the excitation and emission wavelengths were 344 and 478 nm, respectively. Due to the broadness of the emission peak (*33*) and background noise, each peak was fitted to a least-squares parabola (*34*). The experiments were carried out by placing a cuvette with 2 mL of buffer containing 31 μM lipid in the spectrometer and continuously adding enzyme solution to it. In all experiments, 20 mM Hepes containing 0.1 mM EDTA (pH 7.4) was used as a buffer. Between consecutive additions, the solutions were allowed to equilibrate for 1 min, before measuring the intensity. The fluorescence emission spectra were recorded between 300 and 550 nm with excitation and emission bandwidths of 4 nm. All data were corrected for the background intensity of the buffer and for dilution. Measurements were made in a 0.5 cm path length cuvette at a temperature of 30 °C, which is above the transition (liquid-crystalline/fluid state) temperature of DMPC and DMPG membranes.

Monolayer Experiments. Surface pressures during the enzymatic reaction were measured using a magnetically stirred (250 rpm) circular well with a surface area of 31 cm^2 and total volume of 50 mL drilled in Teflon. Surface pressure data were monitored using a KSV5000-3 manufactured by KSV Instruments, Helsinki. The subphase was 20 mM Hepes containing 0.1 mM EDTA (pH 7.4). Lipids were solved in chloroform and were subsequently spread from this solution onto the subphase at an ambient temperature of about 22 °C to an initial pressure of approximately 25 mN/m. The enzyme was then injected below the layers.

Molecular Dynamics Simulations. The high-resolution crystal structure of Hll solved to 1.84 Å resolution was used as the model for the wild-type structure (*1*, *35*). Coordinates were obtained from the Protein Data Bank at Brookhaven (*36*) (entry code: 1tib). The S146A mutant was generated by replacing the active Ser with Ala.

The molecular dynamics simulations were performed using the C version (charged) of the GROMOS force field (*37*). Simulations were carried out in water (4050 molecules; SPC model) applying octahedral periodic boundary conditions. SPC water taken from a liquid equilibrium configuration (*38*) was added to the simulation cell, and 8 water molecules at the lowest electrostatic potential were replaced by sodium ions to neutralize the system (*39*). Each system was equilibrated for 5 ps using a temperature coupling constant of 0.1 ps and a pressure coupling constant of 0.5 ps. The nonbonded pair list was updated every 10 steps, and the nonbonded and long-range electrostatic interactions were truncated at 8 and 10 Å, respectively.[2] The SHAKE algorithm (*43*) was applied to constrain the bond lengths to their equilibrium positions, and the equations of motion were solved using the Verlet algorithm (*44*). Simulations were performed at constant temperature (300 K) with a time step of 2 fs, and coordinates were saved every 0.05 ps. Examination of the molecular structures and analyses of the trajectories were carried out using the WHAT IF modeling program (*45*). The stability of the simulations was checked by computing several geometrical properties (radius of gyration, number of hydrogen bonds, root-mean-square displacement, surface accessibility, number of residues in random coil conformation, number of strained dihedrals). Detailed analyses of these properties indicate that the simulation of the mutant structure was stable over the whole time period, while in the simulation of the wild-type lipase, the polar hinge region Arg81-Ser85 flips over after approximately 500 ps, so that the polar residues are exposed to and interacting with the solvent (data not shown). This flip causes several structural changes, and in particular, the loop regions Asp57-Asp62 and Ala68-Leu75 are affected by the flip. This part of the trajectory was not included in the essential dynamics analyses. The essential dynamics analysis methodology has been described several times in the literature, and a detailed mathematical derivation has appeared in ref *46*. This analysis technique allows separation of protein motions into two classes (*46*−*53*): a low-dimensional essential subspace, in which most of the motions with a large momentum are concentrated, and a high-dimensional near-constraints subspace, in which merely small-amplitude, rapidly equilibrating, Gaussian-like motions occur (*46*, *54*). A useful method for comparing protein motions of 2 simulations on similar systems is the combined analysis technique (*55*). In this methodology, the two trajectories of the wild-type Hll and the S146A mutant are concatenated. The combined trajectory is then used for constructing and diagonalizing the covariance matrix. This diagonalization yields a set of eigenvalues and eigenvectors. Each eigenvector describes protein motions in a certain subspace, which is a part of the total configurational space explored by the protein. The projection of the combined trajectory onto the individual eigenvectors (i.e., the dot product between the combined trajectory and the individual eigenvectors) indicates where the particular motions described by the individual eigenvectors occur along the trajectory. The dot product calculated for each frame is 0, when the motions do not occur in that frame, while the dot product is 1, when the protein motions can be solely described by the chosen eigenvector. The time dependence of the dot product describes the static and dynamic changes, which are reflected in the average value and the mean square fluctuations of the dot product. A large average value of the dot product combined with a low value for the mean square fluctuations indicates that the changes are purely static, whereas a large value for the mean square fluctuations

[2] The effect of truncation of long-range electrostatic interactions has been discussed in the literature (*39*−*41*). The chosen cutoff radius in the present study is based on a recent study, where it has been shown that concerted Cα motions extracted from molecular dynamics simulations using the GROMOS force field were in good agreement with experimental data (*42*).

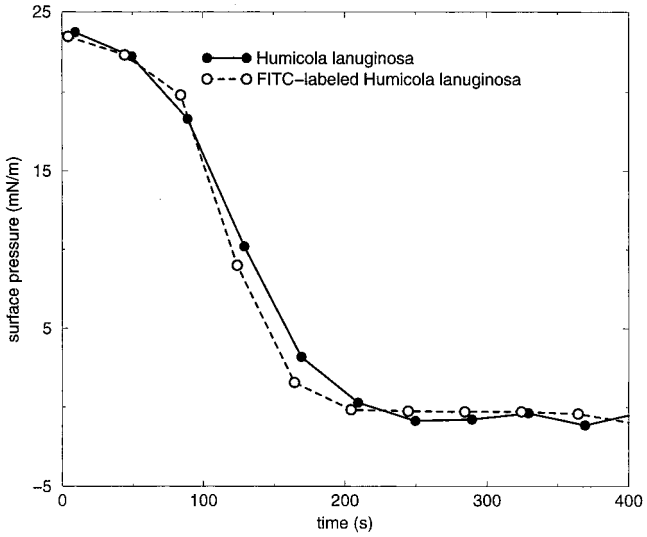

FIGURE 1: Activity of the wild-type Hll and the FITC-labeled Hll against 1,2-*sn*-didecanoylglycerol. Experimental error of the surface pressure is ±5%.

combined with a small average value indicates that the changes are purely dynamic.

RESULTS AND DISCUSSION

Binding to Phospholipid Liposomes. Resonance energy transfer between suitable donor−acceptor pairs provides a sensitive fluorescence method to study lipid dynamics, lipid phase separation, and peripheral ligand−membrane interactions (*56*−*61*). We applied this method to study the binding of the wild-type Hll and the S146A mutant to liposomes of 1,2-dimyristoyl-*sn*-glycero-3-phosphocholine (DMPC) or 1,2-dimyristoyl-*sn*-glycero-3-phosphoglycerol (DMPG). DMPC and DMPG liposomes contained pyrene-labeled lipids 1-palmitoyl-2(pyren-1-yl)decanoyl-*sn*-glycero-3-phosphatidylcholine (bisPDPC) and 1-palmitoyl-2(pyren-1-yl)decanoyl-*sn*-glycero-3-phosphatidylglycerol (bisPDPG), respectively, which were used as fluorescence energy donors. Both lipases were labeled with fluorescein isothiocyanate, which serves as a quencher for the fluorescence of the strongly excimer-forming bisPDPC and bisPDPG lipids. Initial experiments were performed to test the activity of Hll toward DMPC and DMPG and to determine the effect of the FITC labeling. The activity was tested by preparing a liposome/enzyme solution and measuring the fluorescence spectrum every 2 min over a period of 60 min. No change in intensity could be measured (data not shown), indicating that the activity against these substrates is negligible. The influence of the labeling on the activity was tested in monolayer experiments, where 1,2-*sn*-didecanoylglycerol was used as the substrate. Figure 1 shows the surface pressure as a function of reaction time. Within the statistical error, the activity of both enzymes is the same, indicating that the labeling of the enzyme does not significantly influence its activity.

The association of Hll and the S146A mutant are noticeably different for DMPG and DMPC liposomes. As shown in Figure 2, Hll bound more widely than the inactive mutant to both liposomes. At a FITC-labeled lipase concentration of approximately 2 μM, the relative fluorescence intensity (RFI) can be ranked as follows: 55% DMPG (Hll) ⇒ 67% DMPC (Hll) ⇒ 72% DMPG (S146A) ⇒ 80% DMPC (S146A). Though both enzymes show higher binding affinity to PG than to PC, the features of the graphs are significantly different. The association of Hll on DMPG increases linearly with concentration, whereas noticeable features are observed in Figure 2a for the S146A mutant. Between 0.4 and 0.6 μM the RFI remains constant. An estimation of the number of bound lipase molecules (assuming a headgroup size of 60 Å (*62*) and an average liposome size of 80 nm (*31*)) at a concentration of 0.4 μM yields 2−3 molecules/membrane surface. However, the actual number is probably lower, since not all lipase molecules are bound to the surface. The constant RFI suggests that it is energetically unfavorable to add further lipase molecules to the surface. Comparing the size of the enzyme (diameter

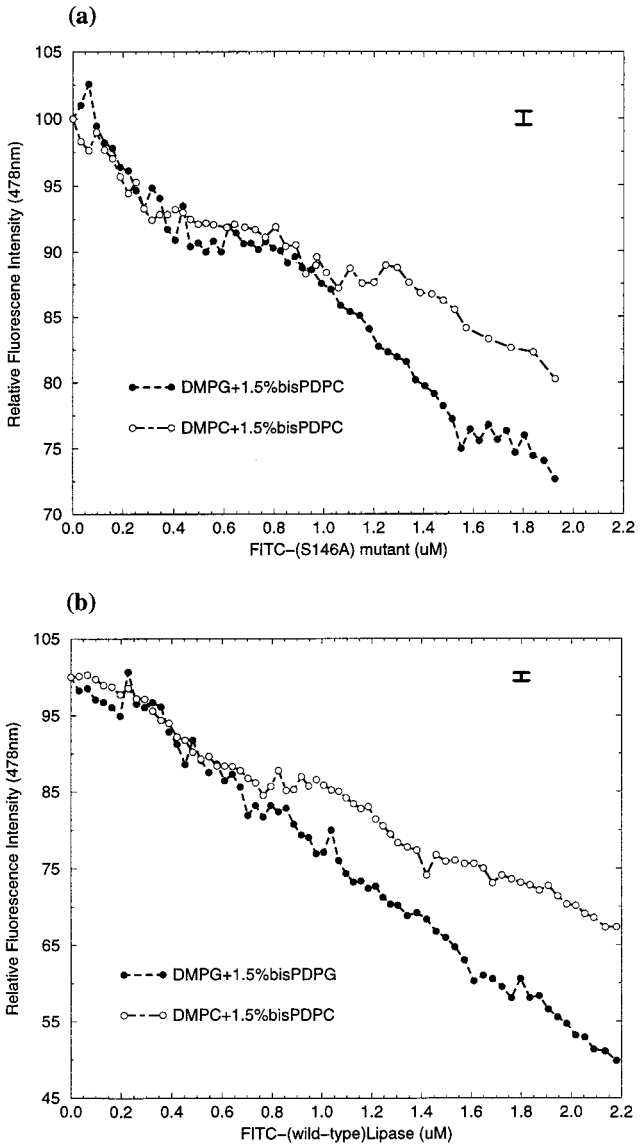

FIGURE 2: Quenching of the pyrene excimer emission as a function of FITC-labeled lipase concentration. Data are shown for (a) the S146A mutant and (b) wild-type Hll. Liposomes are composed of 98.5% 1,2-dimyristoyl-*sn*-glycero-3-phosphoglycerol and 1.5% 1-palmitoyl-2(pyren-1-yl)decanoyl-*sn*-glycero-3-phosphatidylglycerol or 98.5% 1,2-dimyristoyl-*sn*-glycero-3-phosphocholine and 1.5% 1-palmitoyl-2(pyren-1-yl)decanoyl-*sn*-glycero-3-phosphatidylcholine. Exitation and emission wavelengths are 344 and 478 nm, respectively. Estimated error is indicated by the bar at the upper right.

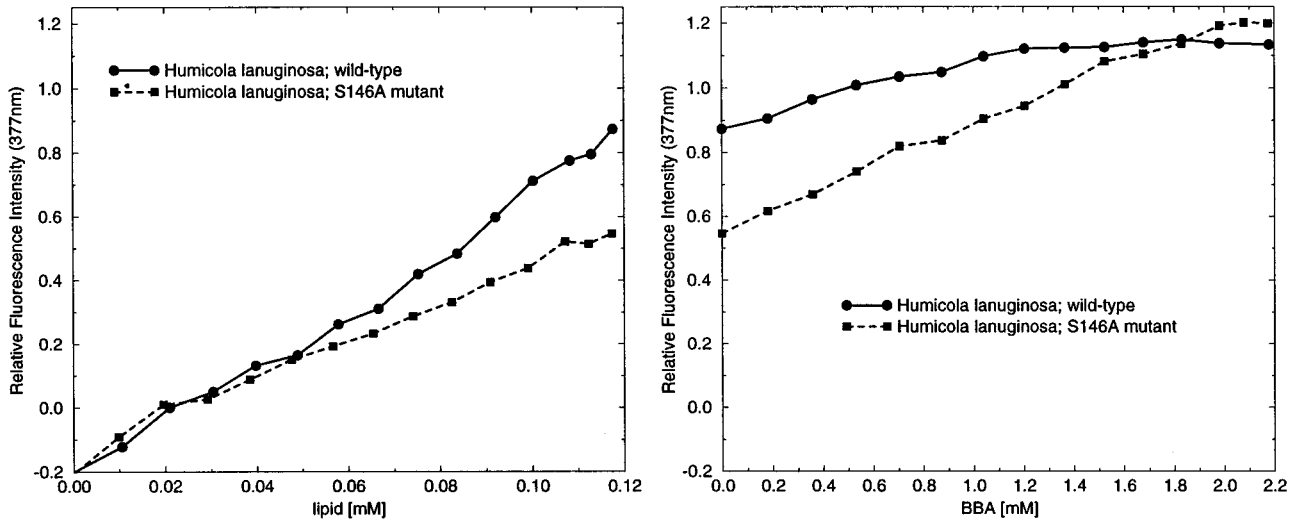

FIGURE 3: Quenching of the pyrene monomer fluorescence as a function of lipid (left) and benzene boronic acid (right) concentrations. Liposomes are composed of 97 mol % DMPG and 3 mol % PDA. Exitation and emission wavelengths are 290 and 340 nm, respectively.

approximately 45 Å) with the size of the liposomes (approximately 800 Å) indicates that steric effects are probably of minor importance. The constant RFI could be due to the ordered arrangement of lipase molecules at the interface ("super-structure" (*63*)). Above 0.6 μM, the concentration of lipase molecules in solution is high enough to overcome the energy barrier and to disrupt the ordered structure of lipase molecules at the membrane surface causing a rearrangement of molecules. Similar effects are observed for the DMPC liposomes, where both Hll and the mutant S146A interact strongly with the DMPC matrix.

These differences suggest that the single mutation perturbs the fluctuations in the active site lid. To further investigate this hypothesis and to elucidate the kinetic properties of the active site lid, we have investigated the effect of benzene boronic acid (BBA) on the binding properties of the two lipases. Boronic acids have been established as potential inhibitors for serine−histidine hydrolases (*64*, *65*) by forming the well-characterized analogue of the tetrahedral intermediate arising in the active site of these enzymes during the course of hydrolysis. The experiments were performed in two steps. First, small amounts of liposomes were continuously added to the enzyme solution and the fluorescence spectra were recorded. At a lipid concentration of approximately 0.12 mM (arbitrarily chosen), increasing concentrations of BBA were added to the solution. Relative fluorescence intensities as a function of lipid and BBA concentration are shown in Figure 3. The affinity of the inactive mutant is smaller than that observed for the wild-type Hll. Addition of boronic acid considerably improves the binding capacity. At 2.2 mM BBA, the pyrene monomer emission for the inactive mutant increases by more than 100%, whereas a much smaller effect is seen for the native Hll, where an increase in the intensity of approximately 25% is observed. As mentioned earlier, upon activation the hydrophobic surface area increases, favoring the binding of the lipase to a lipid interface. Hence, the higher-intensity data measured with the wild-type Hll suggests that more lipase molecules are in the active (open) conformation than observed for the inactive mutant. Binding of BBA molecules to the active site groove forces the lipase molecule to adopt an open conformation, and subsequently due to hydrophobic interactions, a higher binding affinity is observed.

Simulations of Hll and the S146A Mutant. To investigate, if the different binding affinities of the two lipases are correlated to differences in the protein dynamics, we have applied molecular dynamics (MD) simulations.[3] Simulations were carried out for 800 ps using explicit water molecules and applying periodic boundary conditions in the *x*, *y*, and *z* directions. As discussed in the Materials and Methods section, 400 ps of the trajectories was stable as estimated by the evaluation of several geometrical properties. Root-mean-square displacement calculated with respect to the starting structure and accessible surface area as a function of simulation time considered in the analysis are displayed in Figure 4. Both quantities are stable and fluctuating around a constant value.

The trajectories were further analyzed to extract the collective protein motions which are central to the relationship between conformational changes and the biophysical properties of proteins such as activity and binding affinity (*52*). These large-scale motions in proteins can be described in terms of a small number of collective variables, which defines the "important subspace" in which most of the dynamics occur. To extract these motions from the resulting trajectories, we applied the essential dynamics analysis technique (*46*).[4] It has been shown that the essential subspaces frequently contain relevant information about protein motions, which are related to the biological function and to the biophysical properties of proteins (*46*, *47*, *49*−*67*). The basic results of an essential dynamics analysis on lipases have been described elsewhere (*68*), where we have shown that there is a pronounced motion in the active site lid and that, as also found for other proteins, there are only a few essential eigenvectors describing the protein dynamics. To investigate the effect of the point mutation on the

[3] MD simulations are useful for showing high-frequency (10^{-15}−10^{-9} seconds) protein motions, but due to the shortness of achievable simulation times (*48*, *66*), simulations cannot describe large-scale domain motions occurring in the microsecond range or slower (*49*, *50*).

[4] It has recently been shown that this method can extract motions observed in the sampling window but is less reliable on time scales which are not actually sampled (*48*).

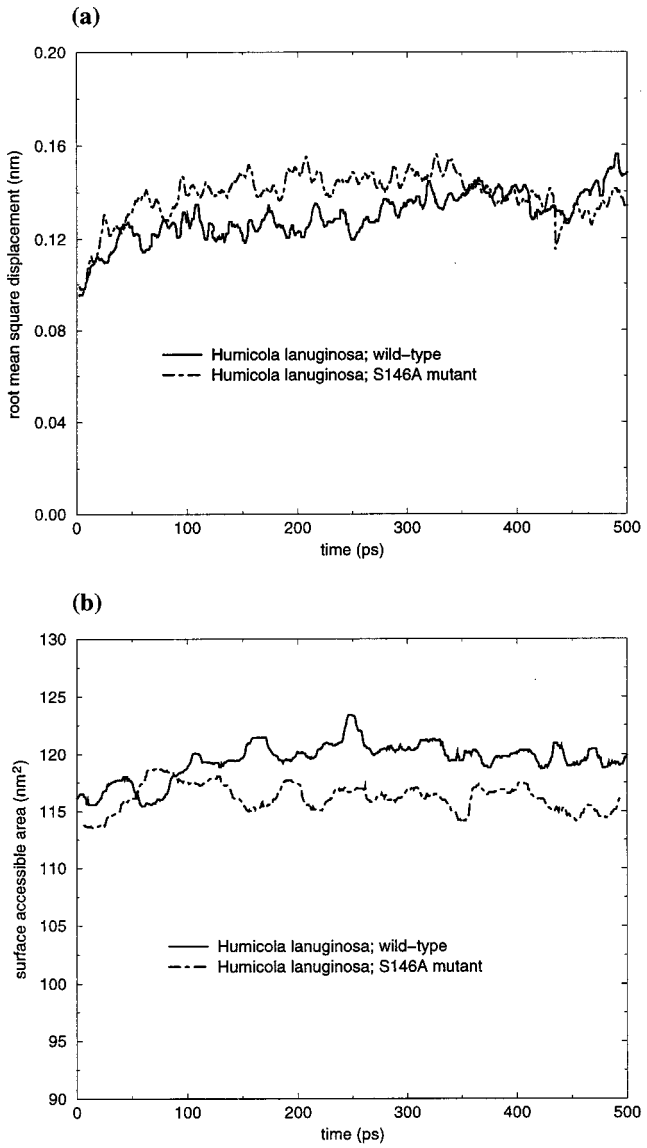

FIGURE 4: Geometrical properties calculated during the simulations of Hll and the S146A mutant: (a) root-mean-square displacement and (b) surface-accessible area as a function of simulation time. Root-mean-square displacement data were calculated between the crystal structure of the wild-type form and the structures obtained during the course of the simulations. Surface accessibility was calculated with the DSSP software (*78*).

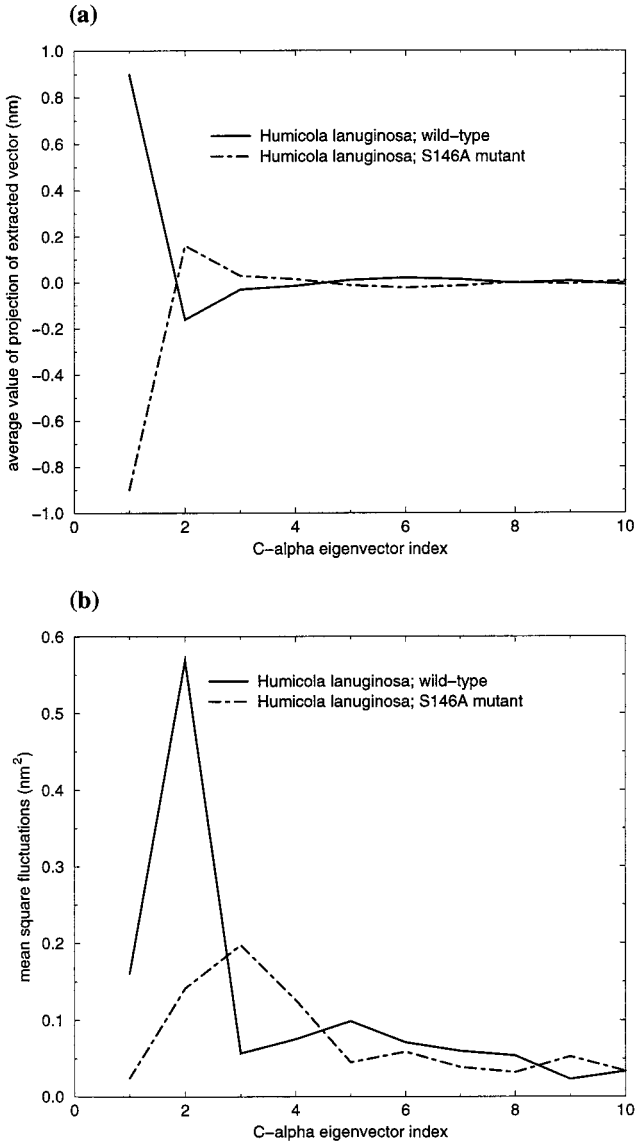

FIGURE 5: (a) Average values of the projections of the extracted vectors obtained from the Cα coordinates covariance matrix of the concatenated trajectories of Hll and the S146A mutant as a function of the eigenvector index. (b) Mean square fluctuations of the values of the projections of the extracted vectors obtained from the Cα coordinates covariance matrix of the concatenated trajectories of Hll and the S146A mutant as a function of the eigenvector index.

dynamics of Hll, we have performed a combined essential dynamics analysis (*55*). As described in the previous section, the analysis is based on the diagonalization of the covariance matrix (*47*), which is constructed from the Cα coordinates of the combined trajectories. This yields a set of eigenvectors and eigenvalues. The eigenvectors represent a direction in a high-dimensional space, describing concerted displacements of atoms. The eigenvalues represent the mean square fluctuations of the total displacement along these eigenvectors. Motions within the subspace can be studied by projecting the combined trajectory onto the individual eigenvectors. This dot product provides information about the time dependence of the conformational changes. In the following paragraph, these structural changes are discussed and specific flexible regions are mentioned. To ease the understanding of the discussion, the secondary structure of the wild-type Hll and the S146A mutant are shown in Figure 7. Relevant segments, which are discussed below, are colored and labeled in Figure 7.

The average value of these projections and the mean square fluctuations in these projections as a function of eigenvector indices is shown in Figure 5, parts a and b, respectively. Significant differences are only observed for eigenvectors <4. Structural changes (static shifts) are reflected in the average value of projection of individual vectors. As shown in Figure 5a, the two curves are symmetrical around 0, since the analysis was performed on the combined trajectories of the two simulations. Structural differences are computed with respect to an average structure, which was calculated from the combined trajectories. The largest average value is observed for eigenvector index 1, and motions along that eigenvector reflect conformational changes in Hll and S146A mutant structures. Visualization of the motions along eigenvector 1 revealed that the structural changes originated

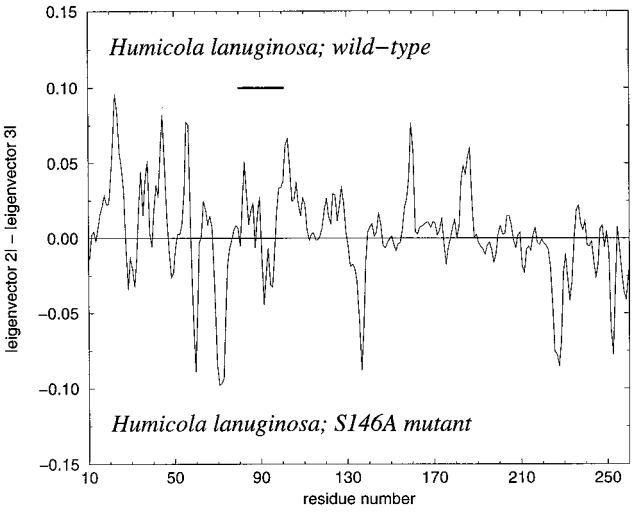

FIGURE 6: Difference between the absolute value of the components of the second and third eigenvectors obtained from the Cα coordinates covariance matrix of the concatenated trajectories as a function of residue number. The solid bar indicates the location of the active site loop.

from a distortion in the hinge region of the active site loop (Gly82-Ser85). This distortion is directly transmitted over the β-sheet to the loop region Glu99-Gly106, which then due to van der Waals contact causes structural changes in the loop region Leu159-Gly163. Differences in protein dynamics are revealed by the mean square fluctuations (Figure 5b). There are notable differences in the motions along eigenvectors 2 and 3. Mean square fluctuations for eigenvector 2 are highest for the wild-type Hll, whereas motions along eigenvector 3 are predominantly observed in the mutant structure (Figure 5b). Visualization of the motions along the different eigenvectors reveals that mutation of the active site has only minor influence on the mobility of residues in the consensus sequence Gly-X_1-Ser-X_2-Gly (where X_1 and X_2 are variable residues). However, fluctuations of the active site lid, the segment Gly31-Asp48, and the segment Asp57-Asp62, which are structurally conserved in lipases from *R. miehei*, *H. lanuginosa*, *Rhizopus delemar*, and *Penicillium camembertii* (*69*, *70*), are significantly different in the native lipase and the S146A mutant. The important role of the loops Gly31-Asp48 and Asp57-Asp62 in the dynamics of the active site lid has also been observed in our previous studies, where we have investigated the effects of solvent polarity and inhibitors on the concerted motions in *R. miehei* lipase (*68*, *69*). Those results indicated that fluctuations in these regions are correlated to the motions of the active site lid. To further quantitate the difference in the fluctuations observed in the wild-type Hll and the S146A mutant, we have calculated the difference between the absolute value of the components of the second and third eigenvectors. The differences as a function of residue numbers are shown in Figure 6 and visualized in Figure 7. The solid bar drawn in Figure 6 indicates the location of the active site lid, which in Figure 7 is viewed from the top. Noticeable differences in the protein flexibility are observed in several regions, and in particular, in the native Hll, both hinge regions are more mobile than in the inactive mutant. In the mutant structure, larger fluctuations are observed in the middle region of the active site lid (segment Trp89-Leu97).

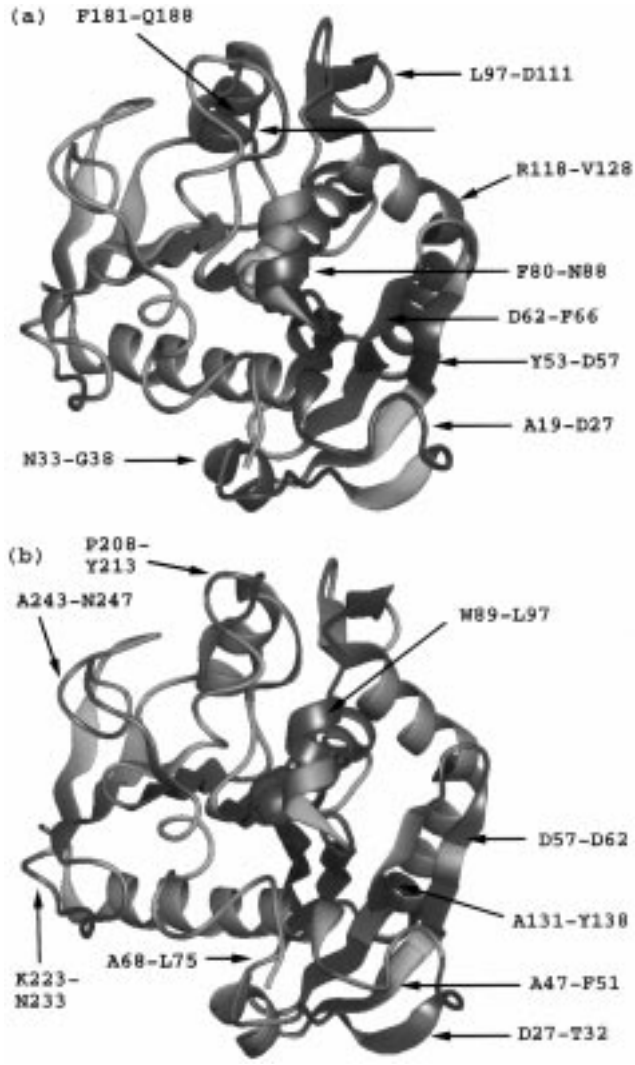

FIGURE 7: Secondary structures of (a) the *Humicola lanuginosa* lipase and (b) the S146A mutant. Both structures are displayed in the closed conformations. The regions labeled and colored blue display flexible segments which are predominately observed in (a) the wild-type *Humicola lanuginosa* lipase or (b) the mutant S146A structures. These regions correspond to the results of Figure 6 and are discussed in the text. Residue 146 is displayed as van der Waals radii and colored yellow in the wild-type Hll (Ser, (a)) or green in the S146A mutant (Ala, (b)).

CONCLUSION

Fluorescence spectroscopy is widely used for studying structure, dynamics, and binding affinities of proteins (*56*, *71*). We have applied this technique to study the binding properties of *H. lanuginosa* lipase and its inactive mutant (S146A). Both enzymes show different binding affinities toward PG and PC matrixes, where in general, Hll shows higher binding affinity to these matrices than the S146A mutant. Though the binding affinity is lower for the inactive mutant, it interacts strongly with the liposomes as indicated by the pronounced features of the relative intensity versus FITC-lipase concentration curves (Figure 2). The results of the molecular dynamics simulations indicate that the binding behavior of the two lipases may be caused by differences in the protein dynamics. Analysis of the trajectories using the essential dynamics technique (*46*) reveals that the motions of several structural elements are influenced by the point mutation. In particular, the active site lid and the conserved

loop regions Gly31-Asp48 and Asp57-Asp62 (*69*, *70*) show different dynamic properties in the two structures. These findings are in accordance with the experimentally observed data. As mentioned earlier, lipase activation involves the displacement of the active site lid allowing the substrate to enter the binding pocket and approaching the active serine. The lid movement exposes previously buried hydrophobic residues and at the same time buries polar residues on the lid helix and on the surface adjacent to it (*12*). The exposure of this hydrophobic patch (*12*, *72*) enhances the interaction with lipid interface and consequently increases the binding affinity. In the simulations, we would not expect to observe a full opening of the lid, since typical motions of peptide loops occur on time scales of $10^{-9}-10^{-1}$ s (*17*−*20*, *73*, *74*). Additionally, Brownian dynamics studies of *R. miehei* lipase revealed that in an aqueous environment the lid does not always open, but it does exhibit some gating motion suggesting that the enzyme molecule may exist in a partially active form (*75*). The present simulations indicate that in the wild-type structure both hinge regions of the active site lid show relatively high flexibility. These fluctuations would support the opening of the lid by a relatively simple, rigid body hinge-type motion (*1*). In the S146A mutant structure, however, the motions are concentrated in the middle region of the lid, which would not allow for a simple hinge-type motion to occur easily and the lid opening is probably less favored. Addition of the transition-state analogue benzene boronic acid (BBA) initially increases the binding affinity of the S146A mutant more effectively than the affinity of Hll. At higher BBA concentration both enzymes yield similar quenching of the pyrene monomer fluorescence, suggesting that a maximum surface coverage of enzyme molecules is reached. At low BBA concentration, the wild-type Hll surface coverage is close to its maximum value and hence only small changes in the relative fluorescence intensity are observed, when BBA is added to the solution. In the case of the S146A mutant, the addition of BBA molecules provides more enzyme molecules in the open conformation, which then due to hydrophobic interactions bind to the liposomes. Our findings highlight the extreme susceptibility of the active site structure even to a very conservative mutation in the protein, such as Ser to Ala. Therefore, small changes can significantly influence the biophysical properties of proteins (*76*, *77*).

ACKNOWLEDGMENT

G.H.P. would like to thank Mrs. Birgitta Rantala for skillful technical assistance. The fluorescence spectroscopy measurements were performed in the Department of Medical Chemistry (Institute of Biomedicine, University of Helsinki, Helsinki, Finland).

REFERENCES

1. Derewenda, U., Swenson, L., Wei, Y., Green, R., Kobos, P. M., Joerger, R., Haas, M. J., and Derewenda, Z. S. (1994) *J. Lipid Res. 35*, 524−534.
2. Brzozowski, A. M., Derewenda, U., Derewenda, Z. S., Dodson, G. G., Lawson, D. M., Turkenburg, J. P., Bjorkling, F., Huge-Jensen, B., Patkar, S. A., and Thim, L. (1991) *Nature 351*, 491−494.
3. Derewenda, Z. S., Derewenda, U., and Dodson, G. G. (1992) *J. Mol. Biol. 227*, 818−839.
4. Derewenda, U., Brzozowski, A. M., Lawson, D. M., and Derewenda Z. S. (1992) *Biochemistry 31*, 1532−1541.
5. Claesson, P. M., Blomberg, E., Frøberg, J. C., Nylander, T., and Arnebrant, T. (1995) *Adv. Colloid Interface Sci. 57*, 161−227.
6. Karplus, P. A. (1997) *Protein Sci. 6*, 1302−1307.
7. Tanford, C. (1997) *Protein Sci. 6*, 1358−1366.
8. Sussman, F., Villaverde, M. C., and Davis, A. (1997) *Protein Sci. 6*, 1024−1030.
9. Goddette, D. W., Christianson, T., Ladin, B. F., Lau, M., Mielenz, J. R., Paech, C., Reynolds, R. B., and Wilson, C. R. (1993) *J. Biotechnol. 28*, 41−54.
10. Dill, K. A. (1997) *J. Biol. Chem. 272*, 701−704.
11. Piéroni, G., Gargouri, Y., Sarda, L., and Verger, R. (1990) *Adv. Colloid Interface Sci. 32*, 341−378.
12. Dodson, G. G., Lawson, D. M., and Winkler, F. K. (1992) *Faraday Discuss. 93*, 95−105.
13. Jain, M. K., Yu, B. Z., and Berg, O. G. (1993) *Biochemistry 32*, 11319−11329.
14. Thuren T. (1988) *FEBS Lett. 229*, 95−99.
15. Muderhwa, J. M., and Brockman, H. L. (1992) *J. Biol. Chem. 267*, 24184−24192.
16. Brockman, H. L. (1984) in *Lipases* (Bergström, B., and Brockman, H. L., Eds.) pp 1−46, Elsevier Science Publishers, Amsterdam, The Netherlands.
17. Kempner, E. S. (1993) *FEBS Lett. 326*, 4−10.
18. Philippopoulos, M., Xiang, Y., and Lim, C. (1995) *Protein Eng. 8*, 565−573.
19. Falzone, C. J., Wright, P. E., and Benkovic, S. J. (1994) *Biochemistry 33*, 439−442.
20. Williams, J. C., and McDermott, A. E. (1995) *Biochemistry 34*, 8309−8319.
21. Peters, G. H., Toxvaerd, S., Larsen, N. B., Bjørnholm, T., Schaumburg, K., and Kjaer, K. (1995) *Nat. Struct. Biol. 2*, 401−409.
22. Peters, G. H., Toxvaerd, S., Olsen, O. H., and Svendsen, A. (1997) *Protein Eng. 10*, 137−147.
23. Holmquist, M., Martinelle, M., Clausen, I. G., Patkar, S., Svendsen, A., and Hult, K. (1994) *Lipids 29*, 599−603.
24. Christensen, T., Woeldike, H., Boel, E., Mortensen, A. B., Hjortshoej, K., Thim, L., and Hansen, M. T. (1988) *Biotechnology 6*, 1419−1422.
25. Favazza, M., Lerho, M., and Houssier, C. (1990) *J. Biomol. Struct. Dyn. 7*, 1291−1300.
26. Nelson, R. M., and Long, G. C. (1989) *Anal. Biochem. 180*, 147−151.
27. TosoHaas, Montgomeryville, PA.
28. Molecular Probes Europe BV, PoortGebouw, Rijnsburgerweg 10, 2333 AA Leiden, The Netherlands.
29. Bradford, M. M. (1976) *Anal. Biochem. 72*, 248−254.
30. Nuclepore, Pleasanton, PA.
31. MacDonald, R. C., MacDonald, R. I., Menco, B. P. M., Takeshita, K., Subbarao, N. K., and Hu, L. (1991) *Biochim. Biophys. Acta 1061*, 297−303.
32. SLM-Amino Inc., Urbana, IL.
33. Kinnunen, P. K. J., Virtanen, J. A., Tulkki, A. P., Ahuja, R. C., and Möbius, D. (1985) *Thin Solid Films 132*, 193−203.
34. Murray, R., and Spiegel, R. (1981) in *Theory and Problems of Statistics*, pp 220−222, Schaum Publ. Company, New York.
35. Lawson, D. M., Brzozowski, A. M., Dodson, G. G., Hubbard, R. E., Huge-Jensen, B., Boel, E., and Derewenda, Z. S. (1994) in *Lipases*—*Their Structure, Biochemistry and Applications* (Woolley, P., and Petersen, S. B., Eds.) pp 77−94, Cambridge University Press, Cambridge, U.K.
36. Bernstein, F. C., Koetzle, T. F., Williams, G. J. B., Meyer, E. F., Brice, M. D., Rogers, J. R., Kennard, O., Shimanouchi, T., and Tasumi, M. (1977) *J. Mol. Biol. 112*, 535−542.
37. Van Gunsteren, W. F., and Berendsen, H. J. C. (1987) *GROMOS: Groningen molecular simulation computer program package*, University of Groningen, The Netherlands.
38. Berendsen, H. J. C., Postma, J. P. M., van Gunsteren, W. F., and Hermans, J. (1981) in *Membrane Proteins: Structures, Interactions and Models* (A. Pullman et al., Eds.) pp 457−

470, Kluwer Academic Publishers, Leiden University, The Netherlands.
39. Fox, T., and Kollman, P. A. (1996) *Proteins: Struct., Funct., Genet. 25*, 315−334.
40. Oberoi, H., Trikha, J., Yuan, X., and Allewell, N. M. (1996) *Proteins: Struct., Funct., Genet. 25*, 300−314.
41. Gilson, M. K. (1995) *Curr. Opin. Struct. Biol. 5*, 216−223.
42. Van Aalten, D. M. F., Conn, D. A., de Groot, B. L., Berendsen, H. J. C., Findlay, J. B. C., and Amadei, A. (1997) *Biophys. J. 73*, 2891−2896.
43. Ryckaert, J. P., Ciccotti, G., and Berendsen, H. J. C. (1977) *J. Comput. Phys. 23*, 327−341.
44. Allen, M. P., and Tildesley, D. J. (1989) in *Computer simulation of liquids*, Clarendon, Oxford, U.K.
45. Vriend, G. (1990) *J. Mol. Graphics 8*, 52−56.
46. Amadei, A., Linssen, A. B. M., and Berendsen, H. J. C. (1993) *Proteins: Struct., Funct., Genet. 17*, 412−425.
47. Ichiye, T., and Karplus, M. (1991) *Proteins: Struct., Funct., Genet. 11*, 205−217.
48. Balsera, M. A., Wriggers, W., Oono, Y., and Schulten, K. (1996) *J. Phys. Chem. 100*, 2567−2572.
49. Elamrani, S., Berry, M. B., Phillips, G. N., Jr., and McCammon J. A. (1996) *Proteins: Struct., Funct., Genet. 25*, 79−88.
50. Marques, O., and Sanejouand, Y.-H. (1995) *Proteins: Struct., Funct., Genet. 23*, 557−560.
51. Garcia, A. E. (1992) *Phys. Rev. Lett. 68*, 2696−2699.
52. Subbiah, S. (1996) in *Protein Motions Molecular Biology Intelligence Unit*, Springer-Verlag, Heidelberg, Germany.
53. Janezic, D., Venable, M., and Brooks, B. R. (1995) *J. Comput. Chem. 16*, 1554−1566.
54. De Groot, B. L., Amadei, A., Scheek, R. M., van Nuland, N. A. J., and Berendsen, H. J. C. (1996) *Proteins: Struct., Funct., Genet. 26*, 314−322.
55. Van Aalten, D. M. F., Amadei, A., Linssen, A. B. M., Eijsink, V. G. H., and Vriend, G. (1995) *Proteins: Struct., Funct., Genet. 22*, 45−54.
56. Kinnunen, P. K. J., Kõiv, A., and Mustonen, P. (1993) in *Fluorescence Spectroscopy* (Wolfbeis, O. S., Ed.) pp 159−171, Springer-Verlag, New York.
57. Mustonen, P., Lehtonen, J., Kõiv, A., and Kinnunen, P. K. J. (1993) *Biochemistry 32*, 5373−5380.
58. Kõiv, A., Palvimo, J., and Kinnunen, P. K. J. (1995) *Biochemistry 34*, 8018−8027.
59. Roberts, G. A., and Tombs, M. P. (1987) *Biochim. Biophys. Acta 902*, 327−334.
60. Rytömaa, M., and Kinnunen, P. K. J. (1996) *Biochemistry 35*, 4529−4539.
61. Kinnunen, P. K. J. (1996) *Chem. Phys. Lipids 81*, 151−166.
62. Möhwald H. (1995) in *Structure and Dynamics of Membranes* (Lipowsky, R., and Sackmann, E., Eds.) pp 161−211, Elsevier, New York.
63. Mustonen, P., Virtanen, J. A., Somerharju, P. J., and Kinnunen, P. K. J. (1987) *Biochemistry 26*, 2991−2997.
64. Vainio, P., Virtanen, J. A., and Kinnunen, P. K. J. (1982) *Biochim. Biophys. Acta 711*, 386−390.
65. Kinnunen, P. K. J., Virtanen, J. A., and Vainio, P. (1983) *Atheroscler. Rev. 11*, 65−105.
66. Clarage, J. B., Romo, T., Andrews, B. K., Pettitt, B. M., and Phillips, G. N., Jr. (1995) *Proc. Natl. Acad. Sci. U.S.A. 92*, 3288−3292.
67. Hayward, S., Kitao, A., and Berendsen, H. J. C. (1997) *Proteins: Struct., Funct., Genet. 27*, 425−437.
68. Peters, G. H., van Aalten, D. M. F., Edholm, O., Toxvaerd, S., and Bywater, R. (1996a) *Biophys. J. 71*, 2245−2255.
69. Peters, G. H., van Aalten, D. M. F., Svendsen, A., and Bywater, R. (1997) *Protein Eng. 10*, 149−158.
70. Derewenda, U., Swenson, L., Green, R., Wei, Y., Dodson, G. G., Yamaguchi, S., Haas, M. J., and Derewenda, Z. S. (1994) *Nat. Struct. Biol. 1*, 36−47.
71. Millar, D. P. (1996) *Curr. Opin. Struct. Biol. 6*, 322−326.
72. Derewenda, Z. S. (1994) *Adv. Protein Chem. 45*, 1−52.
73. Wade, R. C., Davis, M. E., Luty, B. A., Madura, J. D., and McCammon, J. A. (1993) *Biophys. J. 64*, 9−15.
74. Wade, R. C., Luty, B. A., Demchuk, E., Madura, J. D., Davies, M. E., Briggs, J. M., and McCammon, J. A. (1994) *Nat. Struct. Biol. 1*, 63−67.
75. Peters, G. H., Olsen, O. H., Svendsen, A., and Wade, R. C. (1996) *Biophys. J. 71*, 119−129.
76. Wade, R. C., and McCammon, J. A. (1992) *J. Mol. Biol. 225*, 679−696.
77. Zhang, Z.-Y., and Wu, L. (1997) *Biochemistry 36*, 1362−1369.
78. Kabsch, W., and Sander, C. (1983) *Biopolymers 22*, 2577−2637.

BI972883L